Research Article

Two-photon grayscale lithography for free-form micro-optical arrays

TAMARA ADERNEUER, 1,2 D OSCAR FERNÁNDEZ, 1 AND ROLANDO FERRINI 1,*

¹CSEM Center Muttenz, Tramstrasse 99, 4132 Muttenz, Switzerland

Abstract: Compared to standard rotationally symmetric macroscopic optical components, free-form micro-optical arrays (FMOAs), sometimes termed microstructured optical surfaces, offer greater design freedom and a smaller footprint. Hence, they are used in optical devices to deliver new functionalities, enhanced device performance, and/or a greater degree of miniaturization. But their more complex surface shape is a challenge for traditional manufacturing technologies, and this has triggered a substantial effort by research institutes and industry to develop alternative fabrication solutions. Two-photon polymerization (2PP) is a promising additive manufacturing technology to manufacture 3D optical (micro)structures. The manufacturing times involved are, however, often impractically long, especially for the excellent surface quality required for optical applications. Recently, Nanoscribe GmbH has reduced manufacturing times substantially with the introduction of so-called two-photon grayscale lithography (2GL). However, its acceleration potential and consequent impact on surface quality have, to the best of our knowledge, yet to be reported. A direct comparison between 2PP and 2GL indicates that, for the investigated FMOA, 2GL is around five times faster than 2PP and also delivers better surface quality. This study therefore confirms the potential of 2GL to manufacture complexly shaped FMOAs.

© 2021 Optical Society of America under the terms of the OSA Open Access Publishing Agreement

1. Introduction

Free-form surfaces are usually defined as surfaces with no axis of rotational invariance [1]. This characteristic provides a great design freedom and has proven advantageous for numerous imaging and non-imaging optical systems. A greater degree of device miniaturization [2–4], better aberration correction capabilities [5,6], larger field of view [7,8], non-symmetric light distributions [9,10], and higher efficiency [11] are the key aspects driving the shift to free-form optical components.

One particularly interesting category of free-form optical surfaces is so-called free-form micro-optical arrays (FMOAs), also known as microstructured optical surfaces [1]. In addition to the abovementioned advantages enabled by their free-form surface shape, the microscopic nature of FMOAs makes them compatible with large-area replication technologies (such as roll-to-roll, roll-to-plate, and wafer UV imprint), hence enabling cost-effective, high-throughput manufacturing (i.e., industrially relevant) processes. FMOAs are essential components for asymmetric diffusers [12], laser beam—shapers, and homogenizers [13,14]. Moreover, their arrayed nature makes FMOAs especially suitable for applications with other array-based components such as sensors, imagers, and displays [7,15–17].

Traditional fabrication technologies such as thermal reflow, reactive ion etching, or microjet printing [18] have been successfully used to produce spherical or slightly aspherical microlens arrays (MLAs) but are highly isotropic and hence not suitable for the realization of FMOAs. Several manufacturing solutions have been proposed for the manufacture of FMOAs, including laser ablation, grayscale laser lithography, two-photon polymerization (2PP), and ultra-precision micromachining [19–25]. However, despite encouraging progress, manufacturers still face

#440251 Journal © 2021 Received

²Swiss Nanoscience Institute, Klingelbergstrasse 82, 4056 Basel, Switzerland

^{*}rolando.ferrini@csem.ch

important challenges, such as steep surfaces, stringent surface quality demands, and long production times. Consequently, great efforts are currently being made to overcome these limitations and to accelerate the production cycle [26]. Other fabrication methods, including some based on grayscale processes, have demonstrated faster manufacturing times, but are limited in terms of shape complexity, resolution, or surface quality (shape and roughness) [27–33].

The very promising technology 2PP has demonstrated its potential to produce high-quality FMOAs [34,35]. However, the stringent form accuracy and surface roughness specifications required by most optical components demand high spatial resolution, and translate to unacceptably long manufacturing times. This limits the use of 2PP to very small FMOAs (ca. 1 mm²), often much smaller than those required by the application in question. As an alternative, Nanoscribe recently released the Quantum X 3D printer, based on the much faster two-photon grayscale lithography (2GL) technology (described in Section 2.) [36,37].

It has been reported that 2GL improves the surface quality (form accuracy and surface roughness) of MLAs and delivers a faster printing speed [37]. To the best of our knowledge, however, this has been not been reported for FMOAs, which are more demanding to fabricate because of their higher complexity of shape. Furthermore, we are yet to see a detailed comparison of 2PP and 2GL. The present paper makes this direct comparison, reporting on printing time, form accuracy, and surface quality, using an exemplary FMOA design. Nanoscribe Photonics Professional GT and Quantum X 3D printers were used, respectively, for the 2PP and 2GL tests.

The remainder of this paper is organized as follows: In Section 2 we describe 2PP technology as well as the metrology tools we use. In Section 3 we present the surface characterization results and our investigation using an optical bench. Section 4 concludes, while Section 5 contains the authors' acknowledgments.

2. Methods

For this study, we selected an array of densely (100%) packed inverted micropyramids with representative dimensions ($50~\mu m$ height and $250~\mu m$ side length of one inverted pyramid). In contrast to typically demonstrated smooth microstructures, here we selected a design with flat facets and sharp edges, as this is more challenging for 2PP-based technologies. All samples are fabricated using 2GL or 2PP with the Nanoscribe 3D printers Quantum X (2GL) and Photonics Professional GT (2PP). Even though both are based on two-photon polymerization, for simplicity we use the term 2PP only to refer to the Photonics Professional GT, and the term 2GL for the Quantum X.

For all samples the printing resin IP-S (Nanoscribe GmbH) is used. Fabrication with the 3D printer Photonics Professional GT was carried out with the core-shell writing strategy with a writing speed of 40 mm s^{-1} for the contours and this figure was 80 mm s^{-1} for the infill. A laser power of 40% was applied for the contours and 80% for the infill. A 25x magnification objective with a numerical aperture of 1.4 was used. Process specifications and further information on fabrication with the 3D printer Quantum X are available in [38].

The additive manufacturing process 2PP is based on photochemical processes [39]. Femtosecond laser pulses are used to polymerize a photosensitive material and write a design into a liquid resist [40]. The polymerization is only initiated in the focal volume of the laser light, where the intensity is above the material crosslinking threshold, which results in great freedom regarding the shapes that can be realized. Within a single field, the laser beam is steered in the XY direction using fast-moving galvo mirrors and the sample is moved vertically by a high-precision stage. For larger fields, the sample is moved using high-precision XY stages. Samples are thus realized by scanning the resist layer by layer, with the height of the layer corresponding to the vertical resolution of the focal volume of the laser. Then, the unexposed resist is dissolved with a developer and washed off. The technology 2GL additionally allows one to change the size of the

focal volume, the so-called voxel, hence enabling higher accuracy and less scanning, the latter resulting in shorter fabrication times (see Fig. 1).

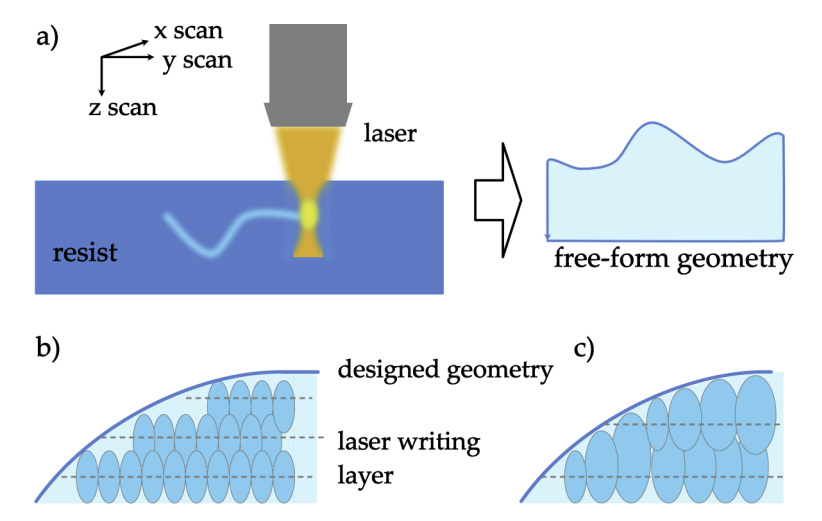


Fig. 1. Two-photon-polymerization fabrication technology. a) A laser beam initiates polymerization in its focal volume. Scanning in lateral and vertical directions, a free-form geometry can be written into the resist. Standard 2PP writes the structure by equal sized voxels (b), whereas the recently developed 2GL allows the size of the voxels to be changed (c). The technology 2GL thus enables higher resolution and fewer layers, which in turn results in shorter fabrication times.

The sample fabricated with 2GL will be referred to as sample 1. Two different writing strategies are included for the samples fabricated with 2PP, one with a small layer thickness, of 200 nm (sample 2), and one with a layer thickness of 2 μ m (sample 3). Sample 2 was chosen as it enables us to compare the highest possible surface quality produced using 2PP with that of sample 1 (produced using 2GL). Sample 3 is included to demonstrate that increasing the layer thickness is not a viable route to reduce the printing time.

The surface characterization is carried out with a confocal (λ = 404 nm) laser scanning microscope (KEYENCE VK-X1100) using 50x and 150x magnification objectives. KEYENCE image stitching mode is used to measure a sample area of 2 × 2 mm² with the 50x objective.

The experimental optical setup for FMOA characterization is presented in Fig. 2. It is used to investigate changes in light distribution linked to a change in surface topology. In the optical

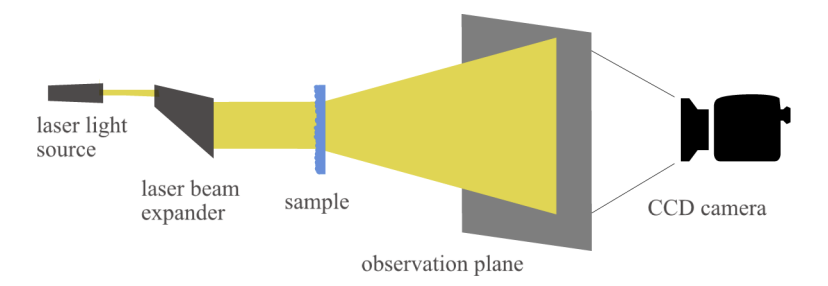


Fig. 2. Schematic sketch of the optical setup, showing the optical bench used to investigate the illuminance distribution resulting from manufacturing deviations. The setup contains a laser light source, a laser beam–expander, a sample, an observation plane, and a CCD camera.

bench, the FMOA under test is uniformly lit by a 532 nm wavelength laser coupled to a beam expander (Thorlabs BE06R/M). The FMOA redistributes the incoming (collimated) light beam through refraction and scattering and produces a certain illuminance distribution on the front face of a distant Lambertian thin-film transmissive surface diffuser (Brightview C-HH80-PE07-HE20, referred to here as the observation plane). A CCD luminance camera (Konica Minolta CA-S25w) records the spatial luminance pattern on the back side of the diffuser. As Lambertian diffusers produce angularly independent luminance, the recorded luminance can be converted into illuminance values through the geometry of the problem. A cage system is implemented to prevent unintentional sample tilt and to facilitate the FMOA-beam alignment. The CCD camera $(980 \times 980 \text{ pixel array})$, placed behind the observation plane, records the luminance distribution over a $19.5 \times 19.5 \text{ cm}^2$ area of the observation plane. The distance between the FMOAs and the observation plane is adjusted to 19 cm to achieve a $19.5 \times 19.5 \text{ cm}^2$ irradiance distribution on the observation plane and hence maximum spatial resolution. The microstructured surface of the samples faces the incoming light beam.

The luminance distribution expected from the nominal FMOA design was predicted using LightTools (version 9.0) raytracing optical simulation software, with the same conditions as those used in the optical setup.

3. Analysis and discussion

Here we present the characterization of the form and roughness of the FMOA samples as well as the optical characterization, carried out in an optical bench. Together these constitute a surface quality analysis of the new fabrication technology.

3.1. Form analysis

The term "form" refers to the overall shape of the surface, including the low spatial frequency components of the surface profile. Form deviation quantifies the deviations of the real surface from the nominal design, excluding the high spatial frequencies. The form deviation analysis is performed as follows: First, the surface topology of the sample is measured (over an area of $2 \times 2 \text{ mm}^2$). The point cloud data, and the nominal design, are imported into the commercial computer software CloudCompare and mutually aligned. Best-fit algorithms minimize the standard deviation of the distance between the point cloud and the 3D CAD model for the best possible alignment. We use the root-mean-square and the peak-to-valley error parameters for free-form surface evaluation [41,42]. The root-mean-square error of sample 1 is $E_{rms} = 5.61 \ \mu\text{m}$, which is calculated from a set of 1330848 measured xyz points. The peak-to-valley error is $E_{pv} = 47.84 \ \mu\text{m}$. For sample 2, the root-mean-square error is $E_{rms} = 3.81 \ \mu\text{m}$ and is calculated from 1331114 measurement points. The peak-to-valley error is $E_{pv} = 40.49 \ \mu\text{m}$. The definitions of the form error parameters are given in [41,42].

The relatively high peak-to-valley errors can be explained by outliers caused, for example, by dust particles on the surface or by edge points that have a larger distance to the edge of the design after alignment. Figure 3 shows the distribution of the point deviations on the surface. Overall the form deviation can be considered quite low, with E_{rms} values in the order of few micrometers.

3.2. Roughness analysis

Surface roughness refers to deviations other than form deviations and includes the high spatial frequencies of the surface profile. It is most often analyzed using line profiles. We therefore use the roughness parameters R_a (mean roughness) and R_q (root-mean-squared roughness) to compare FMOAs fabricated with 2GL and with 2PP, respectively. Details of the roughness definitions can be found in ISO standard 4288 [43,44]. The increasing use of 3D surface characterization instruments, meanwhile, led to areal roughness parameters being included in ISO standard 25178 [45]. We therefore also use the areal parameters S_a (mean roughness value within a defined

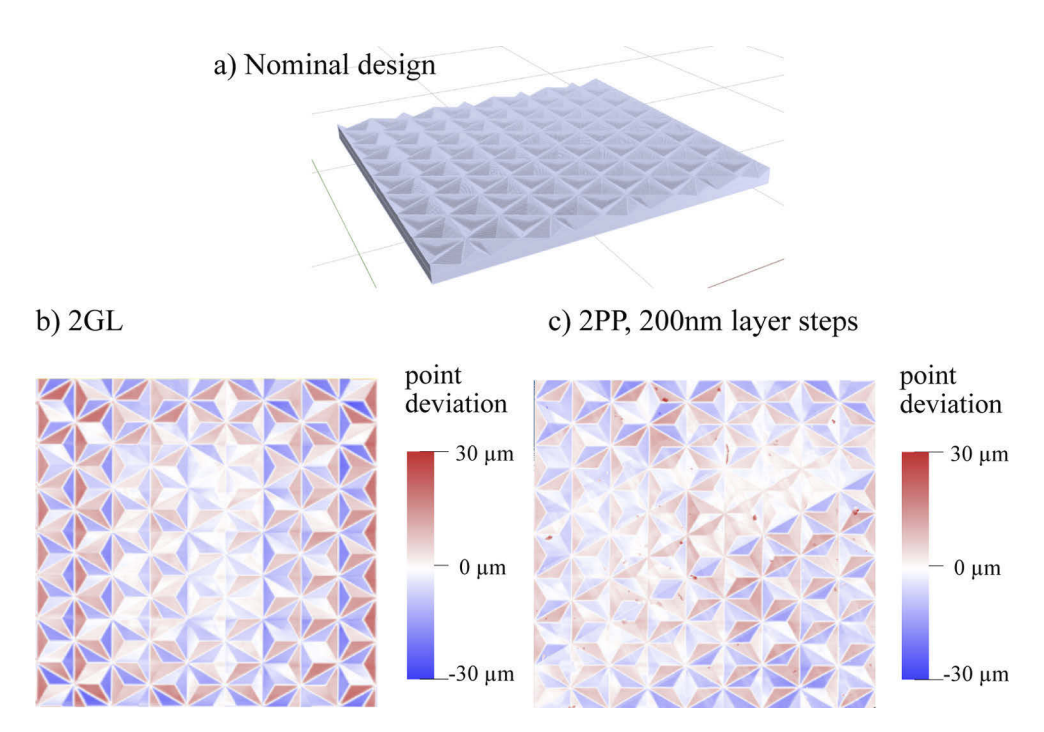


Fig. 3. a) Nominal design and deviations from the nominal design for b) sample 1, fabricated with 2GL, and c) sample 2, fabricated with 2PP. The FMOA samples are characterized with a confocal laser scanning microscope in stitching mode to cover an area of 2×2 mm². The point cloud data is then aligned to the nominal design and the point deviation is calculated and visualized using the analyze tool of the 3D CAD program Rhinoceros.

range) and S_q (squared roughness value within a defined range) to compare the two different technologies.

The profile roughness of sample 1, produced with 2GL, and sample 2, produced with 2PP, are shown in Fig. 4. The calculated profile roughness of sample 1 is $R_a = 12$ nm and $R_q = 14$ nm. Due to the non-planar geometry of the samples, a tilt correction is applied and the values are calculated using the KEYENCE software MultiFileAnalyzer and a cutoff wavelength of $\lambda_c = 80 \ \mu m$. Calculation of the area-based roughness values gives $S_a = 10$ nm and $S_q = 13$ nm for sample 1. An area of $20 \times 20 \ \mu m^2$ was chosen for the analysis, and due to the non-planar form shape correction was applied by waveform removal and by applying a high-pass filter (L-filter, Gaussian) of 25 μm for minimizing long spatial wavelength components.

The analysis of sample 2, fabricated using 2PP, gives a profile roughness of $R_a=36$ nm and $R_q=43$ nm. Analogous to sample 1, tilt correction is applied and calculations are performed using KEYENCE analysis software with six sample lengths and a cutoff wavelength of $\lambda_c=80~\mu\text{m}$. The area roughness calculations are obtained for sample 2: $S_a=29~\text{nm}$ and $S_q=37~\text{nm}$, on an area of $20\times20~\mu\text{m}^2$, with shape correction by waveform removal and a Gaussian high-pass filter (L-filter) of 25 μm .

Comparing the roughness values for the two technologies (see Table 1), sample 1 has lower roughness than sample 2, with a difference of $\Delta R_a = 24$ nm, $\Delta R_q = 29$ nm, $\Delta S_a = 19$ nm, and $\Delta S_q = 24$ nm. It can be concluded that the recently introduced 2GL technology enables the fabrication of optical surfaces with lower surface roughness.

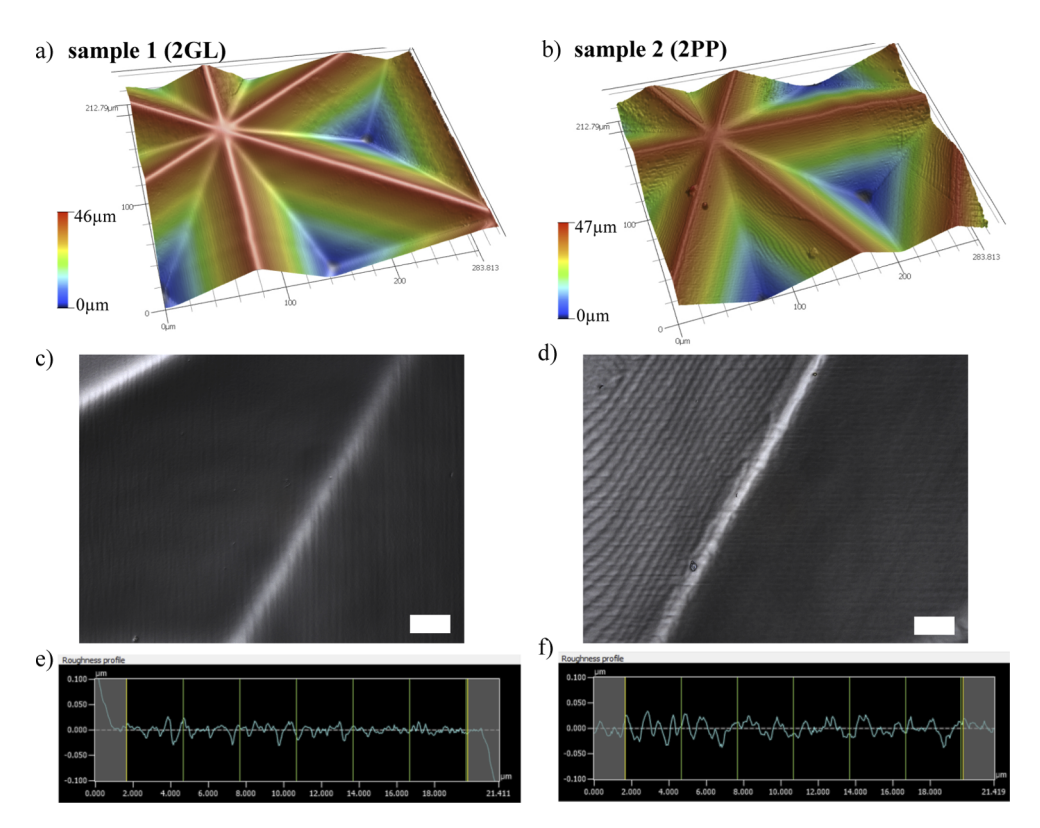


Fig. 4. Roughness characterization with a confocal laser scanning microscope of (a, c, and e) sample 1, prepared with 2GL, and (b, d, and f) sample 2, prepared with 2PP. a) and b) each show a 3D image, in perspective view, of measurements taken with a 50x magnification objective. c) and d) each show an image, in top view, of measurements taken with a 150x magnification objective and the white scale bar corresponding to a length of $10~\mu m$. e) and f) show the respective roughness profiles.

Table 1. Form and roughness results for samples 1, 2, and 3, to compare surface quality results for 2GL and 2PP.

Sample	E_{rms}	E_{pv}	R_a	R_q	S_a	S_q	printing time
No.1 (2GL)	5.61 μm	47.84 μm	12 nm	14 nm	10 nm	13 nm	6.5 h
No.2 (2PP)	3.81 μm	40.49 μm	36 nm	43 nm	29 nm	37 nm	33.5 h
No.3 (2PP)	4.41 μm	32.83 μm	349 nm	412 nm	515 nm	635 nm	3.5 h

3.3. Optical bench characterization

For an additional quality inspection of the microscale form, we apply an indirect optical method using an optical bench. It is not, however, only of interest to investigate the surface topology itself; it is also helpful to quantify the impact of form accuracy on light distribution, which allows a fast and easy comparison of the surface form deviations between samples of the same nominal design. The samples are illuminated by a collimated laser beam and the refracted distribution on an observation plane is recorded (see Fig. 2). This is hence an additional method of surface inspection, as the microscale deviations are linked to a change in the light distribution pattern. Sample 1, fabricated using 2GL, and samples 2 and 3, fabricated using 2PP, are investigated. Sample 2 is fabricated with a high resolution of 200 nm layer height steps, sample 3 with a layer height step of 2 μ m. The illuminance patterns on the observation plane are shown in Fig. 5. The

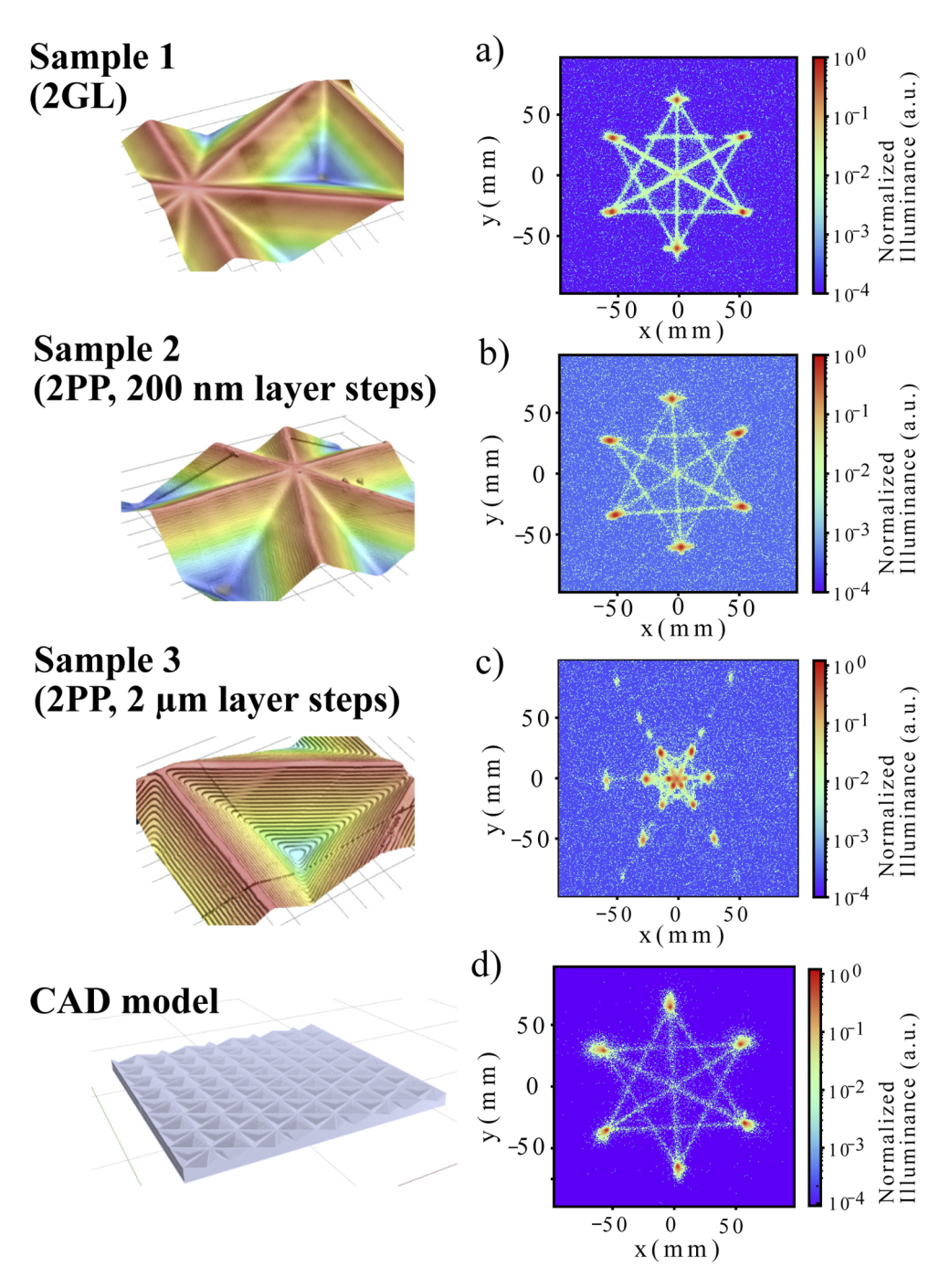


Fig. 5. Experimentally measured relative illuminance patterns of samples 1 (a), 2 (b), and 3 (c). On the left, a three-dimensional characterization image taken with a confocal microscope at 150x magnification is displayed. On the right, the respective measurements in logarithmic scale are displayed. d) Predicted illuminance distribution produced by the nominal design using ray-tracing optical simulations.

performance of sample 3 indicates that reducing the printing time by increasing maximum layer thickness is not a viable option. A sample fabricated using 2PP with a layer thickness of 1 μ m was also tested, and still showed significant deviations in its illuminance pattern compared to the nominal design. Therefore, only samples with a layer thickness of 2 μ m are displayed here. A significant change in light distribution is caused by an increase in layer height. A change of the illuminance pattern can be linked to a change in the surface topology. In order to inspect more closely, the data was analyzed by displaying the light levels in logarithmic scale, which makes features of very low light level visible. Figure 5 shows the light distribution over four orders of magnitude.

The illuminance patterns produced by samples 1 and 2 and the simulated illuminance of the digital CAD model show the same pattern: hexagonally arranged bright spots with lines connecting them. As we obtain the same distribution pattern from sample 1 and from sample 2, even when displaying down to extremely low light levels, it can be concluded that the distributions of samples 1 and 2 are in very good agreement with one another. The simulated pattern is in good agreement with the patterns experimentally obtained from samples 1 and 2. It can thus be concluded that the surface form of each of these samples is thus also in very good agreement with that of the nominal design. Comparing samples 2 and 3, however, one clearly sees a change, in the form of a hot spot appearing in the center and the hexagonal pattern shifting toward the center for sample 3. It can thus be concluded that in order to achieve acceptable optical performance using 2PP technology, thin layer steps are mandatory, which increases the manufacturing time beyond acceptable values. A difference in background illuminance is visible in the illuminance pattern. While the experimental setup was shielded from windows and other light sources in the room, background noise is nevertheless caused by minor variations in the ambient light.

Characterization with an optical bench is a further verification of good surface form quality and is a fast, easy method for inspecting the quality of FMOAs.

4. Conclusion

We have shown that 2GL is a significant advance, decreasing fabrication time compared to 2PP while maintaining excellent form accuracy and surface roughness, even for non-spherical microstructures with planar facets and relatively sharp edges and corners.

Our results were confirmed using illuminance measurements in an optical bench. This indirect optical method can serve as a fast and easy approach to the inspection of the surface quality and form accuracy of FMOAs, as any surface deviation results in a change in the light distribution pattern.

Funding. Innosuisse - Schweizerische Agentur für Innovationsförderung (33436.1 IP-ENG).

Acknowledgments. The authors would like to acknowledge the financial support of Innosuisse, provided via the project FreeMLA (Freeform lens and microlens arrays for high-quality lighting systems, project nr. 33436.1 IP-ENG), and the support of the Institute of Polymer Nanotechnology (INKA) at the University of Applied Sciences and Arts Northwestern Switzerland (FHNW) in fabricating samples using the Nanoscribe 3D printer Photonics Professional GT. We also thank Nanoscribe GmbH for fabricating samples using the Quantum X 3D printer. We want to acknowledge the Nano Imaging Lab for providing access to the confocal laser scanning microscope (KEYENCE VK-X1100).

Disclosures. The authors declare no conflicts of interest.

Data availability. Additional data underlying the results presented in this paper may be obtained from the authors upon reasonable request.

References

- F. Z. Fang, X. D. Zhang, A. Weckenmann, G. X. Zhang, and C. Evans, "Manufacturing and measurement of freeform optics," CIRP Ann. 62(2), 823–846 (2013).
- D. Cheng, Y. Wang, H. Hua, and M. M. Talha, "Design of an optical see-through head-mounted display with a low f-number and large field of view using a freeform prism," Appl. Opt. 48(14), 2655–2668 (2009).
- M. P. Chrisp, B. Primeau, and M. A. Echter, "Imaging freeform optical systems designed with NURBS surfaces," Opt. Eng. 55(7), 071208 (2016).

- 4. Y. Liu, Y. Li, and Z. Cao, "Design method of off-axis extreme ultraviolet lithographic objective system with a direct tilt process," Opt. Eng. 54(7), 075102 (2015).
- 5. W. T. Plummer, "Unusual optics of the Polaroid SX-70 Land camera," Appl. Opt. 21(2), 196-202 (1982).
- L. Xu, K. Chen, Q. He, and G. Jin, "Design of freeform mirrors in Czerny-Turner spectrometers to suppress astigmatism," Appl. Opt. 48(15), 2871–2879 (2009).
- W. Chen, X. Zhang, X. Liu, and F. Fang, "Optical design and simulation of a compact multi-aperture camera based on a freeform microlens array," Opt. Commun. 338, 300–306 (2015).
- Z. Zhuang, Y. Chen, F. Yu, and X. Sun, "Field curvature correction method for ultrashort throw ratio projection optics design using an odd polynomial mirror surface," Appl. Opt. 53(22), E69–E76 (2014).
- R. Mohedano, J. Chaves, and M. Hernández, "Free-form illumination optics," Adv. Opt. Technol. 5(2), 129–136 (2016).
- R. Wu, K. Li, P. Liu, Z. Zheng, H. Li, and X. Liu, "Conceptual design of dedicated road lighting for city park and housing estate," Appl. Opt. 52(21), 5272–5278 (2013).
- J. C. Mi nano, P. Benítez, P. Zamora, M. Buljan, R. Mohedano, and A. Santamaría, "Free-form optics for Fresnel-lens-based photovoltaic concentrators," Opt. Express 21(S3), A494

 –A502 (2013).
- 12. L. Sun, S. Jin, and S. Cen, "Free-form microlens for illumination applications," Appl. Opt. 48(29), 5520–5527 (2009).
- Y. Jin, A. Hassan, and Y. Jiang, "Freeform microlens array homogenizer for excimer laser beam shaping," Opt. Express 24(22), 24846–24858 (2016).
- C. Leiner, W. Nemitz, F. P. Wenzl, and C. Sommer, "Ultrathin free-form micro-optical elements for direct-lit applications with a large distance-height ratio," OSA Continuum 1(4), 1144–1157 (2018).
- W. Yuan, L.-H. Li, W.-B. Lee, and C.-Y. Chan, "Fabrication of Microlens Array and Its Application: A Review," Chin. J. Mech. Eng. 31(1), 16 (2018).
- 16. M.-K. Park, H. Park, K.-I. Joo, T.-H. Lee, K.-C. Kwon, M.-U. Erdenebat, Y.-T. Lim, N. Kim, and H.-R. Kim, "Fast-switching laterally virtual-moving microlens array for enhancing spatial resolution in light-field imaging system without degradation of angular sampling resolution," Sci. Rep. 9(1), 11297 (2019).
- P. Nussbaum, R. Völkel, H. P. Herzig, M. Eisner, and S. Haselbeck, "Design, fabrication and testing of microlens arrays for sensors and microsystems," Pure Appl. Opt. 6(6), 617–636 (1997).
- 18. H. Ottevaere, R. Cox, H. P. Herzig, T. Miyashita, K. Naessens, M. Taghizadeh, R. Völkel, H. J. Woo, and H. Thienpont, "Comparing glass and plastic refractive microlenses fabricated with different technologies," J. Opt. A: Pure Appl. Opt. 8(7), S407–S429 (2006).
- D. Infante-Gómez and H. P. Herzig, "Design, simulation, and quality evaluation of micro-optical freeform beam shapers at different illumination conditions," Appl. Opt. 55(29), 8340–8346 (2016).
- T. Gissibl, S. Thiele, A. Herkommer, and H. Giessen, "Sub-micrometre accurate free-form optics by three-dimensional printing on single-mode fibres," Nat. Commun. 7(1), 11763 (2016).
- T. Gissibl, S. Thiele, A. Herkommer, and H. Giessen, "Two-photon direct laser writing of ultracompact multi-lens objectives," Nat. Photonics 10(8), 554–560 (2016).
- 22. L. Kong, Y. Ma, M. Ren, M. Xu, and C. Cheung, "Generation and characterization of ultra-precision compound freeform surfaces," Sci. Prog. 103(1), 003685041988011 (2020).
- E. Harnisch, M. Russew, J. Klein, N. König, H. Crailsheim, and R. Schmitt, "Optimization of hybrid polymer materials for 2PP and fabrication of individually designed hybrid microoptical elements thereof," Opt. Mater. Express 5(2), 456–461 (2015).
- W.-L. Zhu, F. Duan, X. Zhang, Z. Zhu, and B.-F. Ju, "A new diamond machining approach for extendable fabrication of micro-freeform lens array," Int. J. Mach. Tools Manuf. 124, 134–148 (2018).
- D. Li, Z. Qiao, K. Walton, Y. Liu, J. Xue, B. Wang, and X. Jiang, "Theoretical and Experimental Investigation of Surface Topography Generation in Slow Tool Servo Ultra-Precision Machining of Freeform Surfaces," Materials 11(12), 2566 (2018).
- 26. "PHABULOuS Pilot Line for free-form micro-optics," Accessed: 2021-06-21.
- A. Piqué, "Laser-Induced Forward Transfer of Functional Materials: Advances and Future Directions," J. Laser Micro/Nanoeng. 9(3), 192–197 (2014).
- 28. R. C. Y. Auyeung, H. Kim, S. Mathews, and A. Piqué, "Laser forward transfer using structured light," Opt. Express 23(1), 422–430 (2015).
- R. Kirchner, N. Chidambaram, M. Altana, and H. Schift, "How post-processing by selective thermal reflow can reduce the roughness of 3D lithography in micro-optical lenses," Proc. SPIE 10095, 1009507 (2017).
- 30. A. Grushina, "Direct-write grayscale lithography," Adv. Opt. Technol. 8(3-4), 163–169 (2019).
- 31. Q. Geng, D. Wang, P. Chen, and S.-C. Chen, "Ultrafast multi-focus 3-D nano-fabrication based on two-photon polymerization," Nat. Commun. 10(1), 2179 (2019).
- 32. S. K. Saha, D. Wang, V. H. Nguyen, Y. Chang, J. S. Oakdale, and S.-C. Chen, "Scalable submicrometer additive manufacturing," Science 366(6461), 105–109 (2019).
- V. Hahn, P. Kiefer, T. Frenzel, J. Qu, E. Blasco, C. Barner-Kowollik, and M. Wegener, "Rapid Assembly of Small Materials Building Blocks (Voxels) into Large Functional 3D Metamaterials," Adv. Funct. Mater. 30(26), 1907795 (2020).
- 34. "High-precision cutting-edge refractive microoptics by additive manufacturing | Nanoscribe," Accessed: 2021-08-09.

- 35. T. Aderneuer, O. Fernandez, A. Karpik, J. Werder, M. Marhöfer, and R. Ferrini, "Surface topology and functionality of freeform microlens arrays," Opt. Express 29(4), 5033–5042 (2021).
- 36. "New: Quantum X for the fabrication of highly-precise microoptics," Accessed: 2021-08-09.
- 37. S. Rodríguez, "Redefining Microfabrication of High-Precision Optics," Photonics Views 17, 36-39 (2020).
- 38. "Premium resources: Essential resources to explore your opportunities," Accessed: 2021-10-31.
- 39. F. Sima, K. Sugioka, R. M. Vázquez, R. Osellame, L. Kelemen, and P. Ormos, "Three-dimensional femtosecond laser processing for lab-on-a-chip applications," Nanophotonics 7(3), 613–634 (2018).
- 40. X. Zhou, Y. Hou, and J. Lin, "A review on the processing accuracy of two-photon polymerization," AIP Adv. 5(3), 030701 (2015).
- 41. X. Wen, Y. Zhao, D. Wang, X. Zhu, and X. Xue, "Accurate evaluation of free-form surface profile error based on quasi particle swarm optimization algorithm and surface subdivision," Chin. J. Mech. Eng. 26(2), 406–413 (2013).
- 42. O. Abdulhameed, S. H. Mian, A. Al-Ahmari, and H. Alkhalefah, "Patch and curvature specific estimation of efficient sampling scheme for complex surface inspection," The Int. J. Adv. Manuf. Technol. 110(11-12), 3407–3422 (2020).
- 43. "ISO 4288:1996 Geometrical Product Specifications (GPS) Surface texture: Profile method Rules and procedures for the assessment of surface texture," (1996).
- 44. T. V. Vorburger, H.-G. Rhee, T. B. Renegar, J.-F. Song, and A. Zheng, "Comparison of optical and stylus methods for measurement of surface texture," The Int. J. Adv. Manuf. Technol. 33(1-2), 110–118 (2007).
- 45. "ISO 25178-2:2012 Geometrical product specifications (GPS) Surface texture: Areal Part 2: Terms, definitions and surface texture parameters,".